J Mater Sci (2013) 48:6431–6436
DOI 10.1007/s10853-013-7444-0

Effect of porosity on the crack pattern and residual strength of ceramics after quenching

Yingfeng Shao · Ruiqi Du · Xiaofeng Wu · Fan Song · Xianghong Xu · Chiping Jiang

Received: 27 February 2013 / Accepted: 10 May 2013 / Published online: 18 May 2013

Abstract The effect of porosity on the crack characteristics of ceramics after water-quenching is studied by measuring the cracks in ceramic sheets. The result reveals that the pore volume fraction has a slight effect on the enhancement of thermal shock resistance of ceramics when the porosity ranges from 0 to 20 %, because the length and density of the long crack in porous alumina are always slightly less than that in dense alumina. This result is in agreement with the prediction based on the minimum potential energy principle using experimentally measured data. Moreover, the proportion of the strength reduction in the third regime decreases significantly with increasing porosity, because the strength of unquenched specimens decreases more rapidly than that of quenched specimens with increasing porosity. The results of this study may help to further understand the thermal shock behavior of ceramics.

Introduction

The periodic crack pattern with regular crack spacing and depth caused by uneven shrinkage is a common phenomenon in paints [1], concrete [2], dried mud, and so on [3]. The periodic cracks will also appear in ceramic material because of its inherent brittleness when ceramic material is under severe thermal shock conditions [4], and the mechanical properties of material will be greatly damaged by cracks [5]. Therefore, the study on the crack patterns of ceramics after thermal shock plays a key role in understanding the mechanism of strength reduction [6, 7].

Based on systematic research on thermal shock [8, 9], Hasselman proposed the thermal shock damage theory and provided qualitative theoretical predictions of the crack propagation behavior of the alumina rods under thermal shock. After Hasselman, Bažant and Nemat-Nasser [10–12] studied the stability of propagated thermal shock cracks by using the energy principle, and theoretically discussed the length hierarchy phenomenon. Then Bahr et al. [4, 13, 14] theoretically and experimentally studied the thermal shock crack patterns of a regular array of cracks. However, in the above researches, the spacing between the cracks was assumed rather than determined from the model system. Thus, Jenkins [15] used a method based on minimum potential energy principle to determine the spacing and penetration of a regular array of cracks in the shrinking slabs under changing temperature fields. Our previous numerical simulation study of the thermal shock crack based on minimum energy principle was in good agreement with the experimental and literature results [16]; however, the study was focused on dense ceramics, as for the demand of porous ceramic, it was necessary to consider the influence of the porosity on thermal shock cracks.

In the present study, we experimentally reveal the crack characteristics of the porous ceramic sheet after quenching it in water. By comparing the crack patterns with the numerical result based on minimum potential energy principle, we further point out the influence of porosity on the crack pattern and residual strength.

Y. Shao (✉) · R. Du · F. Song · X. Xu
State Key Laboratory of Nonlinear Mechanics (LNM), Institute of Mechanics, Chinese Academy of Sciences, Beijing 100190, China
e-mail: shaoyf@lnm.imech.ac.cn

X. Wu · C. Jiang
Solid Mechanics Research Center, Beijing University of Aeronautics and Astronautics, Beijing 100191, China

Materials and methods

Materials processing

The porous ceramic studied and reported herein was made of Al_2O_3 powder (particle size 0.5 μm, Xiongdi material Co., Jiyuan, China) and polymethylmethacrylate (PMMA) spheres (particle size 15 μm, Soken chemical Co., Suzhou, China) as pore-forming agent. The mixed powder was uniaxially pressed at 20 MPa into pellets and then isostatically pressed at 150 MPa. The resulting samples were heated at a rate of 1 °C/min to 500 °C to burn away the PMMA and then heated at 10 °C/min to 1650 °C for 2 h. The porosity of ceramics was calculated by measuring dimension and weight, and the value was 1.2, 10.5, 21.3, and 32.0 %, respectively. Thus, the specimens were designated as A1, A11, A21, and A32, respectively, for different porosities. The specimen surface was observed by a scanning electron microscopy (S-570, Hitachi, Tokyo, Japan). The SEM micrographs indicated that sample A1 had the mean grain size of 3.1 μm and sample A11 contained a random distribution of pores decomposed from PMMA, as shown in Fig. 1.

Thermal shock test

The ceramic sheets with dimensions of 1.0 mm in width, 9.8 mm in thickness, and 50 mm in length were employed to investigate the crack patterns after thermal shock by the conventional water-quenching technique. The specimens with different porosities were stacked together so as to be subjected to the same thermal shock loading. In order to prevent the access of coolant to the side faces, the sheet was stacked with another four ceramic slabs, and was bound up with inconel wires (0.4 mm in diameter, Shanghai new Soviet China special alloy material Co., Shanghai, China) positioned <4 mm from the both ends of the slabs, as shown in Fig. 2.

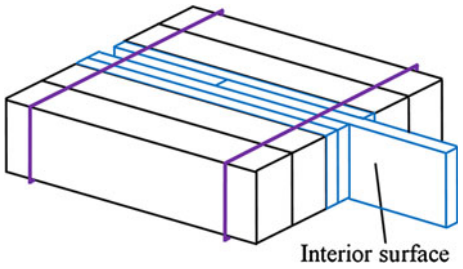

Fig. 2 Stacked samples prepared for thermal shock and the definition of the interior surface of the sheets

The specimens were heated at a rate of 10 °C/min to a preset temperature and held at this temperature for 20 min. After that, the heated specimens were dropped by free fall into a water bath that was maintained at 20 °C with a thermostat for 5 min. Taken out and dried at 80 °C for 2 h, the specimens were then impregnated with a blue dye (Shanghai ink factory, Shanghai, China) for the purpose of observing the cracks that formed during thermal shock. The interior crack patterns were studied by digitally scanning. Four specimens were chosen to examine the length and density of cracks at every temperature difference. Note that the crack patterns appearing within 10 mm from both ends of each specimens were excluded for the sake of eliminating boundary effects.

Mechanical properties

The residual strengths of the quenched specimens were determined in a three-point bending test with a support span of 30 mm and a cross-head speed of 0.5 mm/min. For comparison, the fracture strengths of the unquenched specimens were also measured under the same conditions as those of the quenched specimens, and four specimens were tested to obtain the average strength. A rectangular bar ($36 \times 4 \times 3$ mm^3) was used on a three-point bending fixture with a span length of 30 mm and a cross-head speed of 0.5 mm/min to determine the Young's modulus E from the

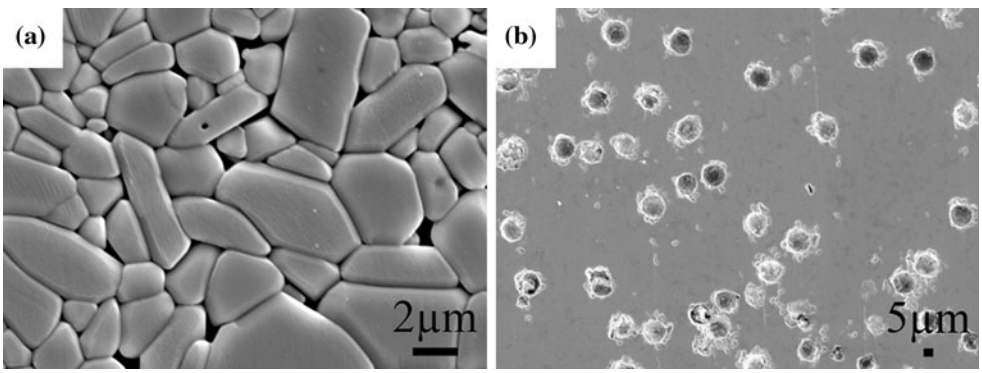

Fig. 1 SEM micrographs showing **a** the grain size on sample A1 surface and **b** the random distribution of pores on sample A11 surface. The mean grain size was measured by linear intercept technique to be about 3.1 μm

stress–strain curves obtained from load vs. deflection plot. The fracture toughness K_{IC} was evaluated by a single-edge notched beam test with a cross-head speed of 0.05 mm/min and a span of 16 mm using $2 \times 4 \times 20$ mm^3 test bars. Thus, the fracture surface energy density γ was determined based on fracture mechanics $2\gamma = K_{IC}^2/E$.

Calculating the extent of crack growth

Here we used minimum potential energy method to calculate the extent of crack growth. The finite element software ANSYS was used for the numerical simulations and the plane stress condition was considered. First, it was assumed that the presence of the cracks that had formed did not influence the temperature distribution in the body under thermal shock. The strain and stress distribution within the body were then calculated from the temperature distribution at any given time. Thus, the total potential of the ceramic material W could be calculated with the elastic strain energy $U = U(s, a, t)$ and the fracture surface energy $S = ar$ caused by uneven temperature distribution and crack formation, respectively:

$$W(s, a, t) = U + S \quad (1)$$

where s and a are the spacing and length of thermal shock cracks, respectively, and t is the time. Thus, the optimal crack patterns that minimize total potential energy on every moment can be obtained by comparing with the different crack patterns. The details are given elsewhere and this approach has provided a good description of cracking in our previous study with dense Al_2O_3 [15, 16].

Results and discussion

The variations in fracture toughness, Young's modulus, and flexural strength values versus porosity are shown in Fig. 3. As indicated, they all decrease with increasing porosity, but the fracture toughness shows less porosity dependence than the strength and Young's modulus, which is similar to those observed elsewhere [6, 17].

The crack patterns that formed in porous ceramics after thermal shock at different temperature differences ΔT are shown in Fig. 4. Cracking is observed when ΔT became >230 K in the samples of A1 and A11, but increases slightly to about 240 K for specimen A21. The increase of critical temperature difference shows that the thermal shock resistance of ceramics increases slightly with porosity but the amount of increase is small, which is very similar to what was reported by Yuan et al. [6] in alumina thermal shock. The number of cracks increases with increasing ΔT in porous ceramics, as shown in Fig. 4; and the crack length seems to increase, indicating the increase

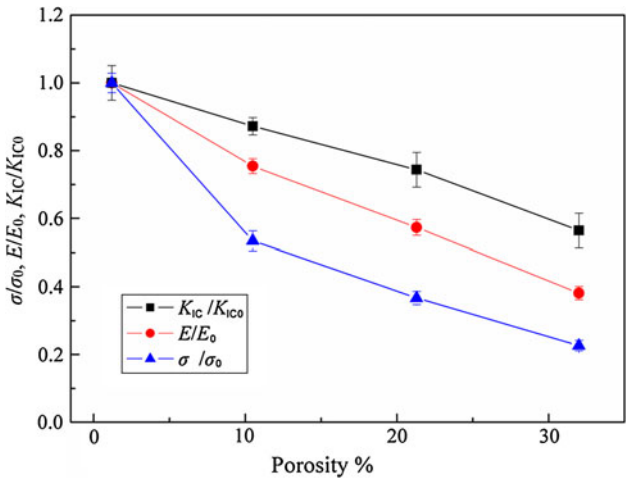

Fig. 3 Relative fracture toughness K_{IC}/K_{IC0}, Young's modulus E/E_0, and flexural strength σ/σ_0 as a function of porosity, where fully dense data as K_{IC0}, E_0 and σ_0 correspond to the data of sample with porosity of 1.2 %

of damage extent. When $\Delta T \approx 680$ K, through-thickness cracks appear in the sheets, which means the complete damage of ceramics. However, when the ceramic porosity is greater than sample A21, the method of impregnating ink is difficult to show crack patterns clearly.

Based on statistical data, we defined the crack >75 % of the longest crack length as the long crack [18]. The variations in length and density of the long crack in porous ceramics with different ΔT are shown in Fig. 5. It reveals that the crack length increases gradually with ΔT in all the ceramics; for example, an increase of 11.7 % is presented from $\Delta T = 280$ K to $\Delta T = 580$ K in the case of sample A21. In addition, the length of long crack in porous ceramic decreases slightly and unnoticeably with increasing porosity at every ΔT; for instance, when $\Delta T = 280$ K, the average crack length of sample A21 is 0.320, which is 5 % shorter than specimen A1 with the crack length value of 0.337. Thus, the pores can act as crack arresters [9]; when a crack reaches a pore, the crack may be forced to alter its path or even stop at the pore.

Like crack length, the density of long crack shows the similar trend with ΔT in porous ceramics; for example, the number of long cracks increases from 44 to 71 (about 1.6 times) of sample A21 with the ΔT ranging from 280 to 580 K. Furthermore, the density of long crack in porous ceramic also decreases slightly with increasing porosity at every ΔT; for instance, when $\Delta T = 280$ K, the number of the long crack of sample A21 is 6 % smaller than sample A1 with the number value of 47. In short, within the porosity range of 0–20 %, thermal shock damage extent gradually decreases with increasing porosity, but the decreased rate is not significant.

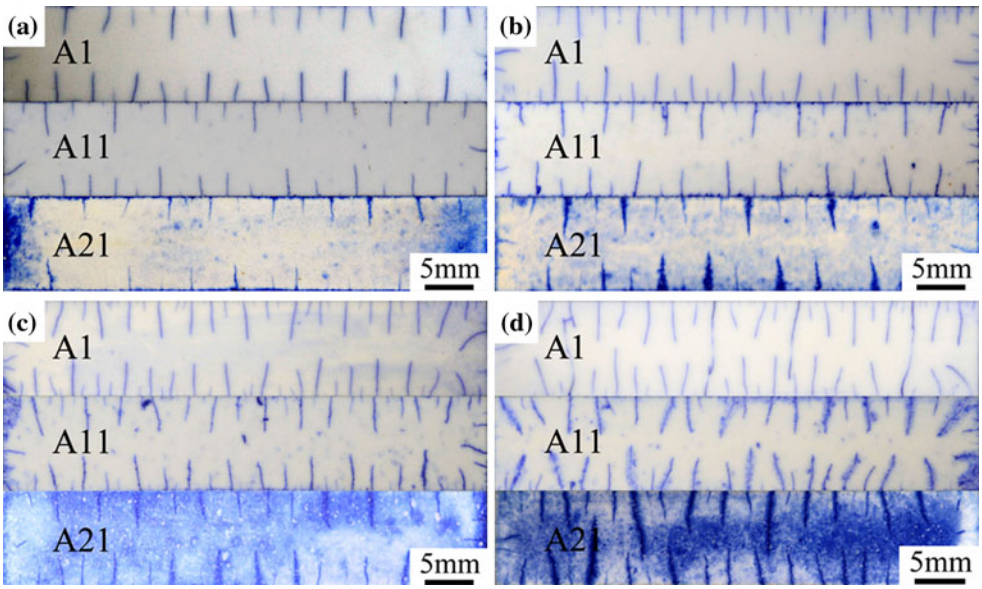

Fig. 4 Thermal shock crack patterns of the ceramic sheets with different porosities quenched in water at ΔT of **a** 280 K, **b** 380 K, **c** 580 K, **d** 680 K

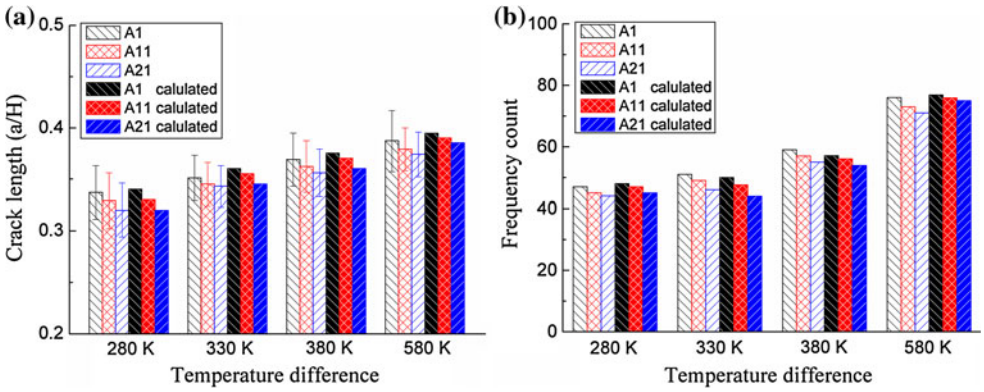

Fig. 5 The variations in **a** length and **b** density of the long crack in porous ceramics with different ΔT and calculated results by minimum energy method, where a is the real crack length and H is the thickness of ceramic sheet

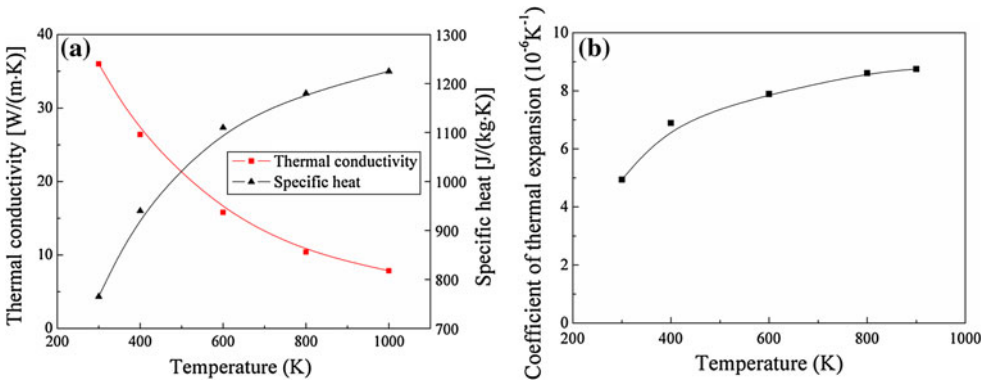

Fig. 6 **a** The thermal conductivity [19], the specific heat [19], and **b** the coefficient of thermal expansion of Al_2O_3 ceramic versus temperature used in calculation [20]

In order to make numerical simulations consistent with the real situation, the thermal conductivity [19], specific heat [19], and thermal expansion coefficient were considered to be temperature-dependent in the range 20–600 °C [20], as shown in Fig. 6. But other physical parameters, such as the Young's modulus, Poisson's ratio, density and fracture surface energy density, were regarded as temperature-independent [16], as shown in Table 1. Within the porosity range of 0–20 %, the thermal expansion coefficient was considered not to vary with porosity in porous

ceramics [21]. The influence of introducing porosity on thermal conductivity k could be calculated through the formula:

$$k = k_0(1-p)^{2.58} \quad (2)$$

where k_0 is the thermal conductivity of the pore-free Al_2O_3 and p is the porosity [22]. Due to the same thermal shock experience, the convective heat transfer coefficient of different porosity alumina could be considered as the same value with ΔT, as shown in Table 2.

The numerical simulations based on minimum energy method precisely predict that the length and number of long crack gradually increase with ΔT, but slightly decrease with increasing porosity at every ΔT, as shown in Fig. 5. The length and number of numerical simulation results are in good agreement with the experimental observations in each ΔT. As a result, the minimum energy method is a very effective method for predicting thermal shock cracks.

Table 1 The values of mechanical properties used in calculation

Specimens	Young modulus, E (GPa)	Poisson's ratio, v	Density, ρ (kg/m^3)	Fracture surface energy density, γ (J/m^2)
A1	370	0.22	3912	19.9
A10	279	0.22	3544	20.6
A20	212	0.22	3117	19.8

Table 2 The convective heat transfer coefficient h of ceramic at different temperatures used in calculation

Temperature (°C)	300	350	400	600
h (W/m^2 K^1)	42000	100000	86000	45000

The strength behavior of porous alumina as a function of quenching temperature difference is shown in Fig. 7. As indicated, the thermal shock behavior of porous ceramics all typically exhibit four stages, because the specimens' strength show an abrupt decrease instead of gradual strength reduction and maintain unchanged in the third regime [5, 8], which is similar to the behavior of dense ceramic in thermal shock test. The proportion of the reduction of strength in the third regime is ranged from 85.9 to 75.3 %, which significantly decreases with increasing porosity, and is quite similar to the behavior of other porous ceramics [23, 24]. The reasons are possibly that the strength of unquenched specimens decreases more rapidly than the fracture toughness with increasing porosity, and that the variation in residual strength (regime III) of specimens has the same trend of the fracture toughness with increasing porosity shown in Figs. 3 and 7, because the measurement methods of residual strength and fracture toughness in this study are very similar with the through-width cracks in specimens shown in Fig. 8. Therefore, the proportion of the strength loss decreases significantly with

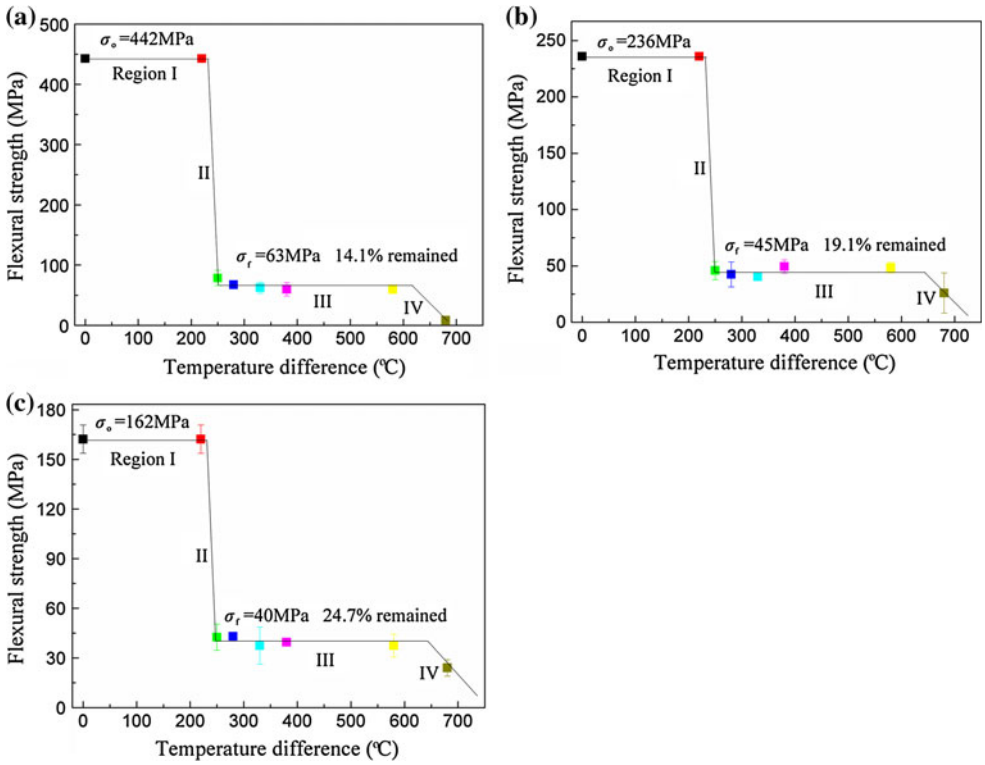

Fig. 7 Strength as a function of quenching temperature difference for alumina sheets of **a** A1, **b** A11, and **c** A21, where σ_0 is the strength of unquenched specimen and σ_f is the residual strength in the third regime

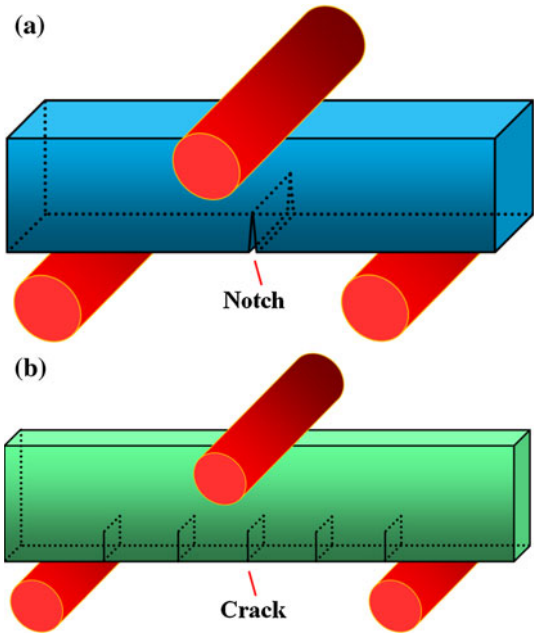

Fig. 8 Schematic diagram of the **a** fracture toughness and **b** residual strength test

increasing porosity. Note that since the length of the long crack decreases slightly with increasing porosity as shown in Fig. 5, it plays a minor role in enhancing the proportion of residual strength [18, 25]. However, despite the fact that proportion of the residual strength is significantly increased with porosity, the strength of porous ceramic, either before or after thermal shock, is less than the dense one.

Conclusions

The thermal shock test of ceramics with different porosities shows that the increase in porosity has a slight influence on the thermal shock behavior of ceramics, such as the critical thermal shock temperature difference and damage extent. The principle of minimum potential energy is used to study the thermal shock crack patterns, and the calculated results are consistent with the experimental observations. Since the strength of unquenched specimens decreases more rapidly than that of quenched specimens with increasing porosity, the proportion of the strength loss in the third regime decreases significantly as the porosity increases. As a result, introducing porosity within the range of 0–20 % is not a good way to enhance the thermal shock properties of ceramics, because the reduction of mechanical properties is large and the promotion of thermal shock resistance is limited.

Acknowledgements This work is supported by the National Natural Science Foundation of China (Grant Nos. 11102208, 91216110, 91016029, 11021262, 11061130550, and 11023001).

References

1. Choules BD, Kokini K, Taylor TA (2001) Mat Sci Eng A 299(1):296
2. Bazant ZP, Kim JK, Jeon SE (2002) J Eng Mech 129(1):21
3. Weinberger R (1999) J Struct Geol 21(4):379
4. Bahr HA, Fischer G, Weiss HJ (1986) J Mater Sci 21(8):2716. doi:10.1007/BF00551478
5. Pompe WE (1993) In: Schneider GA, Petzow G (eds) Thermal shock and thermal fatigue behavior of advanced ceramics. Kluwer Academic Publishers, Dordrecht, p 3
6. Yuan C, Vandeperre LJ, Stearn RJ, Clegg WJ (2008) J Mater Sci 43(12):4099. doi:10.1007/s10853-007-2238-x
7. Vandeperre LJ, Kristofferson A, Carlström E, Clegg WJ (2004) J Am Ceram Soc 84(1):104
8. Hasselman DPH (1970) J Am Ceram Soc 53(9):490
9. Hasselman DPH (1963) J Am Ceram Soc 46(11):535
10. Bažant ZP, Ohtsubo H, Aoh K (1979) Int J Fract 15(5):443
11. Nemat-Nasser S (1978) Int J Eng Sci 16(4):277
12. Nemat-Nasser S, Keer L, Parihar K (1978) Int J Solids Struct 14(6):409
13. Bahr HA, Balke H, Kuna M, Liesk H (1987) Theor Appl Fract Mech 8(1):33
14. Bahr HA, Weiss HJ, Maschke H, Meissner F (1988) Theor Appl Fract Mech 10(3):219
15. Jenkins D (2005) Phys Rev E 71(5):056117
16. Jiang CP, Wu XF, Li J, Song F, Shao YF, Xu XH, Yan P (2012) Acta Mater 60(11):4540
17. Rice R (1996) J Mater Sci 31(8):1969. doi:10.1007/BF00355133
18. Shao YF, Zhang Y, Xu XH, Zhou ZL, Li W, Liu BY (2011) J Am Ceram Soc 94(9):2804
19. Bergman TL, Lavine AS, Incropera FP, Dewitt DP (2011) Fundamentals of heat and mass transfer. Wiley, Hoboken, p 987
20. Jiang DL, Li LT, Ouyang SX, Shi JL (2006) In: Shi CX, Zhong QP, Li CG (eds) China materials engineering canon. Chemical Industry Press, Beijing, p 35
21. Ashby MF (2005) In: Scheffler M, Colombo P (eds) Cellular ceramics structure, manufacturing, properties and applications. Wiley, Weinheim, p 9
22. Wagh A (1993) J Mater Sci 28(14):3715. doi:10.1007/BF00353169
23. Shen L, Liu M, Liu X, Li B (2007) Mater Res Bull 42(12):2048
24. She J, Yang J, Ohji T (2003) J Mater Sci Lett 22(5):331
25. Jin ZH, Feng YZ (2009) J Therm Stress 32(5):431